Ceramics International xxx (xxxx) xxx

Contents lists available at ScienceDirect

Ceramics International

journal homepage: www.elsevier.com/locate/ceramint

Structural and *in vitro* biological evaluation of sol-gel derived multifunctional Ti^{+4}/Sr^{+2} co-doped bioactive glass with enhanced properties for bone healing

Amirhossein Moghanian [a,*], Saba Nasiripour [b], Zahra Miri [c], Zeinab Hajifathali [d], Seyed Hesamedin Hosseini [a], Mohammad Sajjadnejad [e], Roozbeh Aghabarari [a], Noushin Nankali [a], Amir K. Miri [f,g], Mohammadreza Tahriri [h]

[a] Department of Materials Engineering, Imam Khomeini International University, Qazvin, 34149-16818, Iran
[b] School of Metallurgy and Materials Engineering, Faculty of Engineering, University of Tehran, Tehran, Iran
[c] Department of Materials Engineering, Isfahan University of Technology, Isfahan, 84156-83111, Iran
[d] Division of Biomedical Engineering, Department of Life Science Engineering, Faculty of New Sciences and Technologies, University of Tehran, Tehran, Iran
[e] Department of Materials Engineering, School of Engineering, Yasouj University, Yasouj, Iran
[f] Biofabrication Lab, Department of Mechanical Engineering, Rowan University, Glassboro, NJ, 08028, United States
[g] School of Medical Engineering, Science, and Health, Rowan University, Camden, NJ, 08103, United States
[h] Department of Engineering, Norfolk State University, Norfolk, VA, 23504, USA

ARTICLE INFO

Keywords:
A. sol-gel method
D. Bioactive glass −58S
D. Strontium
D. Titanium

ABSTRACT

The principal focus of this study was to evaluate the effect of different strontium (Sr) percentages substitution (Sr content = 0, 1, 3, 6, 9, and 12 mol. %) and fixed 5 mol. % titanium (Ti) in bioactive glass (T-BG) in terms of *in vitro* biological, bactericidal, and structural behaviors of SiO_2-60%, CaO-(31-x)%, P_2O_5-4%, TiO_2-5%, SrO-X% (mol. %) TS-BG. The structural analysis of BGs specimens containing Ti and Sr was performed by scanning electron microscopy (SEM), X-ray diffraction (XRD), Energy-dispersive X-ray spectroscopy (EDS), Fourier transform infrared spectrum (FTIR), Transmittance electron microscopy (TEM), and Inductively coupled plasma-atomic emission spectroscopy (ICP-AES) analyses. The alkaline phosphatase (ALP) activity test and 3-(4,5dimethylthiazol-2-yl)-2,5-diphenyltetrazolium bromide (MTT) analysis were also conducted to investigate *in vitro* biological behavior of TS-BGs. Meanwhile, the bactericidal efficiency of TS-BGs against MRSA was examined.

The SEM results indicated that hydroxyapatite (HA) appeared on TS-BGs' surface after one and two weeks of immersion in the simulated body fluid (SBF). HA characteristic peaks in XRD patterns as well as *P*–O and C–O bands in FTIR spectra confirmed the *in vitro* bioactivity. A similar trend in altering MC3T3 cell proliferation and cell differentiation was observed by increasing Sr amount up to 6 mol. %. Then, it had a downward trend up to 12 mol. % Sr. Meanwhile, the more Sr amounts added, the more TS-BGs antibacterial activity was achieved, and the specimen with 12 mol. % Sr and fixed 5 mol. % Ti (TS12) showed 34.27% bactericidal efficiency more than the control specimen (TS0). Taken together, the specimen with 6 mol.% Sr and fixed 5 mol. % Ti (TS6) was chosen as an optimal specimen among the other synthesized TS-BGs because of its higher *in vitro* bioactivity (HA forming ability after 7 days), MC3T3 cell proliferation, differentiation, and bactericidal efficiency than other specimens.

1. Introduction

Tissue engineering (TE) has emerged as an applied and integrated field that aims to design and induce new biological substitutes and integrate with biological cells for regenerating and improving damaged tissues [1]. The cells, biomaterials, and factor therapy are indeed used to grow and modify the living cells to replace or repair tissues damaged because of a genetic disorder, different kinds of diseases, or trauma [2].

* Corresponding author.
E-mail address: moghanian@eng.ikiu.ac.ir (A. Moghanian).

https://doi.org/10.1016/j.ceramint.2021.07.113
Received 23 April 2021; Received in revised form 23 June 2021; Accepted 13 July 2021
Available online 14 July 2021

Biomaterials also promote cell proliferation and attachment, which lead to regenerating and forming bone. Therefore, biomaterials play a fundamental role in this field [3–5]. They can further provide an extracellular matrix for bone regeneration as scaffolds. In fact, they have been able to contact cells and blood and be replaced by hard and soft tissues [6–9]. One type of biomaterials is bioactive glass (BG), which has emerged as a glass-ceramic for bone tissue engineering (BTE) applications. Moreover, BGs should be able to accomplish some criteria. To be more precise, they should be able to enhance cell proliferation, activity, and adhesion. Moreover, not only should they be biocompatible but also not lead to cytotoxicity. Furthermore, stimulate osteogenesis and promote bone regeneration should be one of their abilities [10–12]. The BG can also bond to the bone through hydroxyapatite (HA) formation on the BG surface.

Larry Hench et al. invented the first BG many years ago to bond to bone and stimulated osteogenesis [13–15]. Also, there are different types of BG like 58S [16], 68S [17,18], as well as 77S [19]. Additionally, the ability of HA formation on BGs' surface [20], bone-forming, regenerating [21], regulator biodegradability [22], and bactericidal activity [23,24] make BGs a promising candidate in the BTE field. Moreover, there are different methods for BGs' synthesis; (i) melt-quench technique, (ii) sol-gel method. The latter is considered to be more simple and easy when compared to the melt-quench [25]. The sol-gel method is fast to apply and easy for a wide range of synthesized compounds [25,26]. Nowadays, BGs have broader applications in medical fields such as regeneration and repair of bone [27], filling space as filler [28], and eye prothese or improves the function of jaw bone and teeth [29,30]. Various amounts of magnesium (Mg) [31], silver (Ag) [32], zinc (Zn) [33], lithium (Li) [34], copper (Cu) [35], titanium (Ti) [36], and strontium (Sr) [37] have been combined with BG in various cases. For example, titanium (Ti) is considered a high biocompatible ion with a broad applications, such as surgical equipment, joint replacement, and dental implants [38,39]. Interestingly, the previous study reported that titanium oxide could improve some properties like antibacterial and photocatalytic [40]. It is noteworthy that the effect of Ti on the cell viability, cell proliferation, and bioactivity properties was investigated [41,42]. In addition, Moghanian et al. introduced the positive individual effect of substituted Ti in 58s-BG in terms of biological and structural properties [43]. Additionally, strontium with the symbol of Sr in the periodic table often replaces Ca because of its similarity in bone formation and highly reactivity [44]. Moreover, Sr is also recognized as an influential therapeutic element to stimulate the generation of bone [45]. It has been reported that the incorporation of Sr in BGs promoted mechanical and bioactivity properties [46]. Also, the impact of Sr on osteoblast and osteoclast cells was previously investigated and the research revealed that Sr led to an increase and decrease in the activity of osteoblast and osteoclast cells, respectively [47,48].

Different diseases put the human body in danger of some problems like infection. Also, many people exposures to bacteria risk and are infected annually. On the one hand, infection plays an inhibited role in most surgeries. On the other hand, Methicillin-resistant *Staphylococcus aureus* (MRSA) is recognized as a severe bacteria that commonly has been the cause of infection especially skin infection [49]. Since it is highly resistant against antibiotics, selecting MRSA as tested bacteria has been challenging [50]. Therefore, modified BGs have been introduced as an effective solution for this issue due to their biocompatible and positive response [41,47,51]. The goal of antibacterial assays on BGs was to measure their response when in contact with selected bacterias [52–54]. Many investigations were already reached from substituted SrO with CaO in different kinds of BGs. However, the reported results have not been the same, and there were some contradictions. On the one hand, some investigations stated the negative effect of Sr on bioactivity efficiency [55–57], while other studies did not affirm this result about *in vitro* bioactivity [58,59]. Some studies confirmed that by increasing Sr amount, cell proliferation increased, followed by it decreased in all incubation times [10,55]. In contrast, in another one, the silicon-based 45S5-BG that Ca was substituted with 0, 10, 50, and 100% Sr, in which it was illustrated that by increasing the amount of Sr and time after culture, the cell proliferation increased. Both these factors (Sr content and time) were reported as influential [56]. Also, an incremental cell proliferation trend was previously reported [57]. It is noteworthy that in some research, the ALP activity of BG containing Sr [60, 61] was first upward and then downward while; in others, it increased and then continued with a steady rate [60,62].

We aimed to analyze the simultaneous impact of Ti with an amount of fixed 5 mol. % and Sr in the range of 0–12 mol. % on structural, biological, and bactericidal efficiency of 58S-BG, which was derived by a sol-gel method and containing SiO_2-60, CaO-(31-x), P_2O_5-4, TiO_2-5, SrO-X (mol. %) (X = 0, 1, 3, 6, 9, and 12 mol. %). Furthermore, in order to characterize co-doped Ti and Sr in bioactive glass (TS-BG) structure, some assays such as, scanning electron microscopy (SEM), X-ray diffraction (XRD) analysis, Energy-dispersive X-ray spectroscopy (EDS) analysis, and Fourier transform infrared spectrum (FTIR), Transmittance electron microscopy (TEM), and inductively coupled plasma-atomic emission spectroscopy (ICP-AES) were done to appraise *in vitro* bioactivity of synthesized TS-BG through monitoring the HA formation on TS-BG surfaces. Besides, alkaline-phosphatase (ALP) test 3-(4,5dimethylthiazol-2-yl)-2,5-diphenyltetrazolium bromide (MTT) assay and antibacterial efficiency analyses were performed to evaluate the biological property. The optimal composition of synthesized TS-BG with the highest efficiency in TE and the biomedical application was then discussed.

2. Materials and methods

2.1. Materials

To synthesize TS-BGs with formula SiO_2-60, CaO-(31-x), P_2O_5-4, TiO_2-5, SrO-X (mol. %) (where X = 0, 1, 3, 6, 9, and 12 mol. %), some primary materials such as tetraethyl orthosilicate ($Si(OC_2H_5)_4$ -TEOS, Merck), calcium nitrate tetrahydrate ($Ca(NO_3)_2$ $4H_2O$, Merck), triethyl phosphate ($(C_2H5)_3PO_4$ -TEP, Merck), tetraethyl orthotitanate ((C_2H_5O) 4Ti (TEOT), St Louis, Mo, Sigma-Aldrich) and strontium nitrate ($Sr(NO_3)_2$, Sigma-Aldrich) were purchased. Additionally, after forming 1-cm-diameter discs and 0.3 g weight specification, the mentioned specimens were soaked in the simulated body fluid (SBF) for specified times and then used for *in vitro* analyses [61].

2.2. TS-BGs synthesis

For the synthesis of TS-BGs powder, nitric acid with the amount of 0.1 N and distilled water were mixed and stirred for 45 min. Followed by TEOS and TEP added separately. TEOT and $Sr(NO_3)_2$ were then added. After adding each of the materials, the solution was stirred for 45 min and to obtain a homogeneous solution, 1 h stirring was required. Additionally, after synthesizing the solution, three steps were required to change the solution to powders. Firstly, the solution was poured in a beaker and enclosed with mesh foil to protect the solution from pollution, and to remove water, they were maintained at room temperature for 72 h. Secondly, to complete the water evaporation, the beaker was heated at 80 °C for 3 days. Lastly, the process of calcination was done at

Table 1
The composition of synthesized TS-BGs in mol. %.

Bioactive glass	Lable	SiO_2	CaO	P_2O_5	TiO_2	SrO
58S–5%TiO_2–0%SrO	TS0	60	31	4	5	0
58S–5%TiO_2–1%SrO	TS1	60	30	4	5	1
58S–5%TiO_2–3%SrO	TS3	60	28	4	5	3
58S–5%TiO_2–6%SrO	TS6	60	25	4	5	6
58S–5%TiO_2–9%SrO	TS9	60	22	4	5	9
58S–5%TiO_2 –12%SrO	TS12	60	19	4	5	12

700 °C for 72 h to remove residual nitrate and water. All synthesized TS-BGs compositions are exhibited in Table 1.

2.3. Characterization of T/S-BGs specimens

2.3.1. Oxygen and bioactive glass density measurement

To calculate the oxygen density of TS-BGs, the below formula was used [63]. According to the formula, The X and the M are the mol fraction and atomic mass of components in the composition, respectively. Furthermore, ρ (the density of TS-BG) was measured by the liquid displacement method.

$$\rho_O = M_O \times (2X_{SiO2} + X_{CaO} + 5X_{P2O5} + X_{TiO2} + X_{SrO}) / [X_{SiO2}M_{SiO2} + X_{CaO}M_{CaO} + X_{P2O5}M_{P2O5} + X_{TiO2}M_{TiO2} + X_{SrO}M_{SrO}]$$

$$\times \rho_{glass}^{-1}$$

2.3.2. X-ray diffraction analysis (XRD)

To investigate the appearance of HA on BGs surface, the X-ray diffraction test was applied on TS-BGs with an X-ray source (Cu-Kα radiation) at 40 kV and in a range of 10°–60°.

2.3.3. Fourier-transform infrared spectroscopy analysis (FTIR)

The FTIR spectroscopy (Nicolet, NEXUS 670) was performed on TS-BGs to evaluate different and efficient changes in the wavelength range of 400–4000 cm^{-1} (by the 8 cm^{-1}resolution).

2.3.4. Energy-dispersive X-ray spectroscopy (EDS), scanning electron microscopy (SEM), and transmittance electron microscopy (TEM)

The scanning electron microscopy (SEM) analysis was done by MIRA3-TESCAN (Czech) apparatus to consider and detect the formed HA on the TS-BG surface after one week and two weeks of soaking in the SBF solution. Additionally, the EDS was carried out to detect the different elements in the structure of HA. Moreover, transmittance electron microscopy (TEM) was performed to confirm the *in vitro* bioactivity.

2.3.5. Inductively coupled plasma-atomic emission spectroscopy (ICP-AES) and pH measuring

The ICP-AES determined the presence and ion release rate of various elements such as Ca, Si, P, Ti, and Sr in TS-BGs structure after soaking in the SBF solution for duration 1, 3, 7, and 14 days. Besides, the value pH variation of TS-BG specimens was measured by (Corning pH-meter- 340, USA) at the end of each specific soaking period in the SBF solution.

2.4. Biological investigation

2.4.1. Alkaline phosphatase (ALP) activity and MTT assay

MTT and ALP tests were performed on TS-BGs to investigate the cell proliferation and osteoblastic activity of MC3T3-E1 cells, respectively. In addition, the living cells and the constructor's suggestions (BioCat, Heidelberg, Germany) cause decreasing tetrazolium salt to formazan crystals in the MTT and ALP assays. Additionally, the MC3T3-E1 cells with 1×10^4 cells/cm^2 density cultured in 24-well plates in the condition involved the humidified atmosphere, 37 °C temperature for one and two weeks, and for the amount of *p*-nitrophenyl liberated, the enzyme activity was fixed at 410 nm [64].

2.4.2. Antibacterial studies

The Antibacterial activity 58S-BGs substituted with Sr and Ti against MRSA with a dilution amount between 0.5×10^8 and 2×10^8 ml^{-1} was evaluated [39,65]. For culturing the MRSA bacteria, at first, 10 mg TS-BGs particles were added to tubes with 1.5 ml Eppendorf, and then the medium was added (0.9 ml LB) and stirred for 60 s. Afterward, the next step was the addition of 0.1 ml bacterial suspension into each Eppendorf tube, which was done before culturing at 37 °C for 1 h. In the last step, after dilution, 100 μl suspensions were plated onto LB-agar plates and immersed in a dark place for one night at 37 °C [39]. Hence, the antibacterial efficiency was measured using the final colony-forming units per milliliter (CFU/mL) [39,65,66].

3. Results and discussion

3.1. Oxygen density (OD)

The presence of additive elements to BG can alter the glass network [67]. Ti and Sr can also affect network connectivity, oxygen density [63], and solubility [68]. According to the ionic radius of Ca (100 p.m.), Ti (68 p.m.), and Sr (113 p.m.), the substitution of Ti with Ca led to the compactness of the BG network because of the smaller ionic radius of Ti than Ca, resulting in an increase in oxygen density and decrease in solubility. In contrast, the substitution of Sr to Ca had a diverse effect on the oxygen density, and it decreased. Moreover, the solubility and ion releasing were enhanced by increasing Sr amounts in the BG composition. Table 2 exhibits the oxygen density of TS-BGs, and Fig. 1 displays the variation of the oxygen density with different SrO contents in TS-BGs. As shown in Fig. 1, the oxygen density of TS-BGs, with a fixed 5 mol. % Ti and different amounts of Sr, was decreased. Ti and Sr separately led to an increase and decrease of oxygen density due to their lower and higher radius ion compared to the Ca's. Additionally, Ti and Sr's simultaneous effect on oxygen density was conceived. The results demonstrated that the oxygen density amount of consequent the simultaneous effect of Ti and Sr on TS-BGs was between the oxygen density amounts of BGs when Ti and Sr were added separately. It was then confirmed that in silicon-based 58S-BGs when SrO substituted with CaO, the addition of Sr to composition led to a decrease in oxygen density of BGs [63]. Hence, additive elements to the composition can alter BG's oxygen density. In fact, the amount of its change corresponds to the ionic radius and the percentage of the additive elements. Besides, the simultaneous effect of fixed 5 mol. % and different amounts of Sr (mol. %) led to a decrease in the oxygen density of TS-BGs, which is shown in Table .2.

3.2. XRD analysis

The XRD analysis was performed to confirm the HA formation on TS-BGs surface, and Fig. 2 shows the immersion result of TS0 and TS6 before and after (1 and 2 week(s)) soaking in SBF solution. The TS-BGs showed two peaks ascribed to 2 thetas (25.8° and 31.8°) that corresponded to the formation of crystalline HA on the TS-BG surface in agreement with the standard JCPDS (No. 09–432) [69]. It is noticeable that there are no HA characteristic peaks in the patterns before immersion (see Fig. 2). The HA peaks appeared after one week immersion and became more pronounced after two weeks. In addition, the Sr content affected the intensity of peaks related to HA, and by enhancing the Sr content, the peak intensity almost diminished. Furthermore, the peak intensities were higher in TS0 (control specimen) than TS6. Moreover, It has been reported that in sol-gel derived substituted 58S-BG, Sr free-BG displayed intense HA characteristic peaks in comparison to BG containing Sr [10]. Also, Hoppe et al. [70] found that BG without Sr exhibited sharper HA peaks in comparison to BG containing different amount of Sr percentage (0, 1, 2.5, and 5 wt %). In another research, Oliveria et al. [62] confirmed that substituted diverse low amounts of Sr (0, 0.5, 1, 1.5 wt %) in HA coating had the same effect on decreasing the peaks intensity, while HA coating containing no Sr showed higher characteristic peaks intensity. Besides, Capuccini et al. demonstrated that when Sr substituted into HA structure, the peak patterns changed and became broader than Sr-free HA. As a conclusion, peaks can become broader by increasing the amount of Sr substituted into HA structure [57]. Altogether, our obtained XRD results were in well agreement with the previous results and showed the sharpest characteristic peaks corresponding to the HA formation for TS0.

Table 2
The oxygen density of TS-BGs.

TS-BGs	TS0	TS1	TS3	TS6	TS9	TS12
Oxygen density	0.77±0.007	0.768±0.006	0.7637±0.005	0.7575±0.004	0.7512±0.003	0.75±0.002

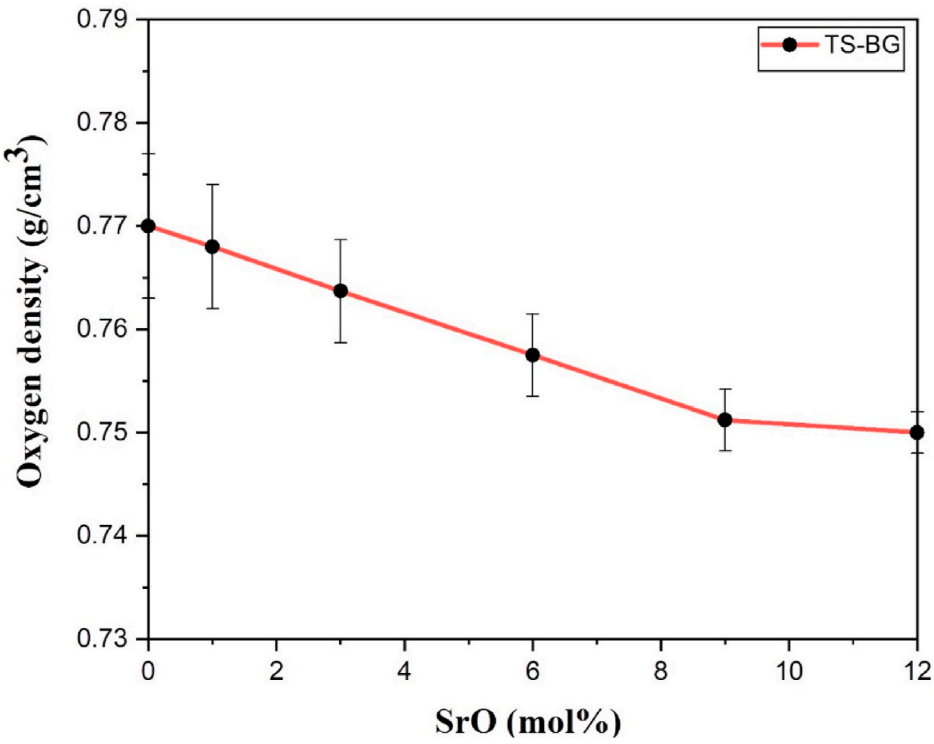

Fig. 1. The oxygen density of all synthesized TS-BGs.

3.3. FTIR evaluation

Fig. 3 presents the obtained results of FTIR transmittance spectra for TS0 and TS6 after one week and two weeks days soaking in the SBF solution. As it was apparent before immersion, no HA peaks were observed. While the *P*–O and C–O peaks attributed to HA formation were seen after immersion in the SBF. In other words, the formation of HA in the specimen with Sr was prolonged compared to the Sr-free specimen. In fact, the Sr retarded the formation of HA on BGs surface, and XRD patterns confirmed it. It was exhibited the C–O as well as *P*–O bands around 1455 cm^{-1}, 870 $cm^{-1,}$ and 570 cm^{-1}, 603 cm^{-1}, respectively. Additionally, the peak near 1250 cm^{-1}, (1000–1100) cm^{-1}, and 470 cm^{-1} belonged to Si–O–Si (vibration mode), peak at 790 cm^{-1} attributed to Si–O (symmetric stretching), and the OH group appeared at 1651 and 3500 cm^{-1}. According to other previous results, Hoppe et al. [70] stated that the C–O and *P*–O stretching bands appeared in (570, 600) cm^{-1} and (1420, 1500) cm^{-1}, respectively, in flame-spray derived BG containing 0, 1, 2.5, and 5 mol. % Sr. Furthermore, Wu et al. [60] observed that the peaks near 860 and 1450 cm^{-1} were attributed to C–O stretching in FTIR spectra. Also, some peaks appeared in 470 and 1076 cm^{-1}, which corresponded to the asymmetric stretching vibration of Si–O–Si. Moreover, it was reported that the C–O and *P*–O banding that attributed to HA formation appeared after 3 days soaking in TS0, whiles it happened after one week of soaking for 58S-BG with 5 and 10 mol. % Sr [10]. Besides, it was reported that by enhancing Sr in the range of 1–5 mol. % in BG that substituted with fixed 3 mol. % Ti, the spectra intensity decreased [55]. In addition, Fig. 4 is shown the under curve area of FTIR spectra of TS0 and TS6 specimens in different ranges from 1070 to 1140 cm^{-1} after 14 days of soaking in the SBF solution. It should be noted that the ratio peaks at 1070 and 1140 cm^{-1} illustrated the HA maturity. The under-curve areas of TS0 and TS6 were measured after normalizing the data, and the results were 0.60 and 0.58, respectively. It showed that the specimen containing Sr amount prolonged the formation of HA and decreased the under curve area compared to specimen free Sr. Moreover, According to previous research, Faraly et al. [71] investigated that increasing the ratio of peaks at 1070 and 1140 cm^{-1} showed the maturity of HA. Furthermore, Moghanian et al. stated that the sol-gel derived 58S-BG with Sr and Li elements in the composition have retard the formation of HA on the BG surface [63]. In other words, the formation of HA in specimens with Sr was prolonged compared to specimens without Sr. In fact, the Sr retarded the formation of HA on BGs surface, and XRD patterns confirmed it.

3.4. SEM

The SEM and EDS results of TS0 and TS6 are presented in Fig. 5. According to Fig. 5, the agglomerate HA was obvious in TS-BGs after one and two weeks of soaking in the SBF solution, and the EDS result confirmed the presence of elements in the composition. The formed HA amount was more remarkable in two weeks than one week in all TS-BGs, and on the 14th day, the TS-BGs surfaces were fully covered by HA globules. Moreover, the SEM results revealed that the amount of HA formed was more significant in TS0 than TS6 with higher Sr amounts because of retarding the HA formation by Sr's presence in specimens. Besides, Fig. 6 shows the TEM image of TS6 before and after immersion in the SBF solution for two weeks. It should be noted that it was not observed any crystalline HA on the BG surface before immersion. While, the HA globules (average diameter equal 80 nm) were observed on the

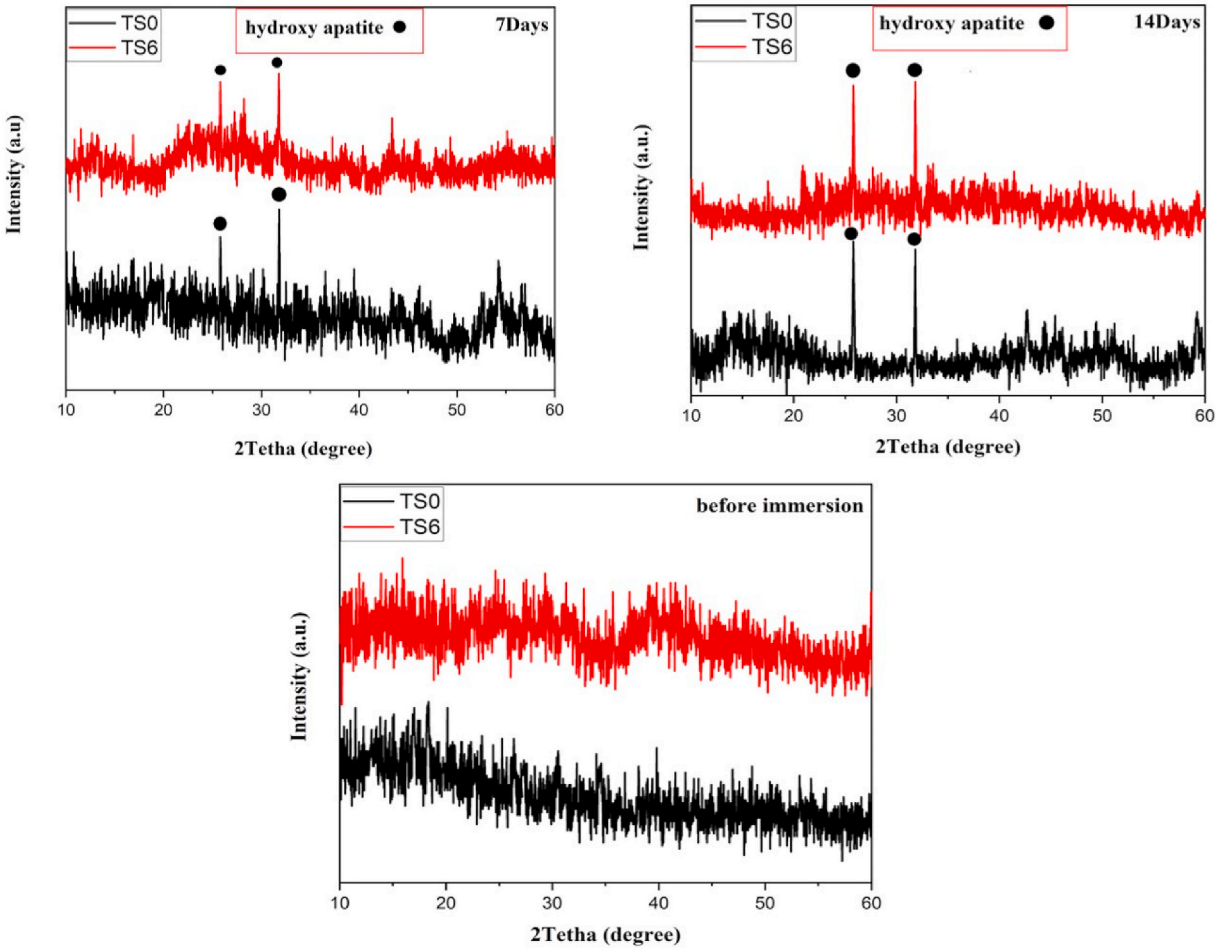

Fig. 2. The XRD patterns of TS0 and TS6 before and after soaking in the SBF solution for one and two weeks.

BG surface that was a confirmation for the SEM results. According to other research, Goel et al. [72] reported that Sr's presence in BG altered the morphology and amount of HA formation on BG surface, i.e., increasing Sr percentage decreased the bioactivity. Moreover, Aina et al. [73] observed that in Sr-substituted HA, Sr's addition in different levels (2, 4 mol.%) into composition changed the morphology and structure during soaking and also led to a decrease in the crystalline degree of specimens. On the other hand, Hoppe et al. evidenced that substitution Sr in flame-spray derived 53S BG, inhibited the HA crystallization and decreased the crystallite size and crystallinity degree [70]. In addition, based on SEM image results, Oliveria et al. [62] noticed that the Sr percentage amount directly affected the thickness of formed HA in Sr substituted HA coating. In all specimens, free Sr HA coating was the thickest, whiles a coating containing 1.5 mol. % Sr displayed the fewest thickness of HA.

It should be noted that the reason for the negative effect of Sr on the bioactivity of BGs could be proved because of the ion radius of Sr (113 ppm), which is more than Ca (100 ppm). Therefore, by substituting CaO with SrO, the unit cell size increased by expanding the unit dimension, which led to decreased crystallinity. Hence, the Sr substitution in BG retarded the formation of HA, and by increasing Sr amount, this effect became more significant. Therefore, it can be concluded that TS0 had higher *in vitro* bioactivity and more formed HA when compared to other TS-BGs specimens.

3.5. ICP analysis

The ICP-AES was performed to evaluate the ion release rate in composition. Also, Fig. 7(a)-(e) displays ions changes after 0, 1, 3, 7, and 14 days immersion in the SBF solution. The Si and Ca ions had a similar trend in TS-BGs. On the first day of immersion, a decrease rate was observed, but it did not prolong, and then the ion release rate decreased until two weeks. Interestingly, the P ions had a reverse behavior. In all periods, the release rate was diminished by different speeds, which could be attributed to the formation of HA during the immersion time. Our results suggested that the presence of Sr in TS-BGs altered the amount and rate of release of Sr ion. In other words, the release of Sr ions was high in the first 3 days of immersion, but it diminished with enhancing time of immersion up to two weeks that attributed to the formation of HA. The maximum and minimum release of Sr ion were attributed to TS1 and TS12 that were 2 and 28 ppm after 1 day immersion, 5 and 60 ppm after 3 days immersion, 7 and 69 ppm after one week immersion, and 7 and 67 ppm after two weeks immersion. Moreover, by increasing the Sr, the ion release amount increased. On the other hand, the Sr had a diverse effect on ions release and decreased Ti ions releasing by increasing the Sr percentage in BGs composition. In previous research, Sr (5, 10 mol. %) effect on sol-gel derived ternary 58S-BG was investigated [10]. Also, it was reported that by increasing Sr amount, the P ions concentration was diminished because of HA formation on the BG surface. However, the number of released P ions increased by increasing Sr amount by immersion periods [10]. Additionally, Hesaraki et al. confirmed that the Ca concentration increased rapidly after 2 days of immersion for sol-gel derived Sr-free 58S glass and after 4 days for Sr-incorporated BG. Meanwhile, the rate of Ca releasing diminished after 3 days for Sr free BG and 4 days for BG containing Sr, respectively, probably due to HA globules utilized the Ca

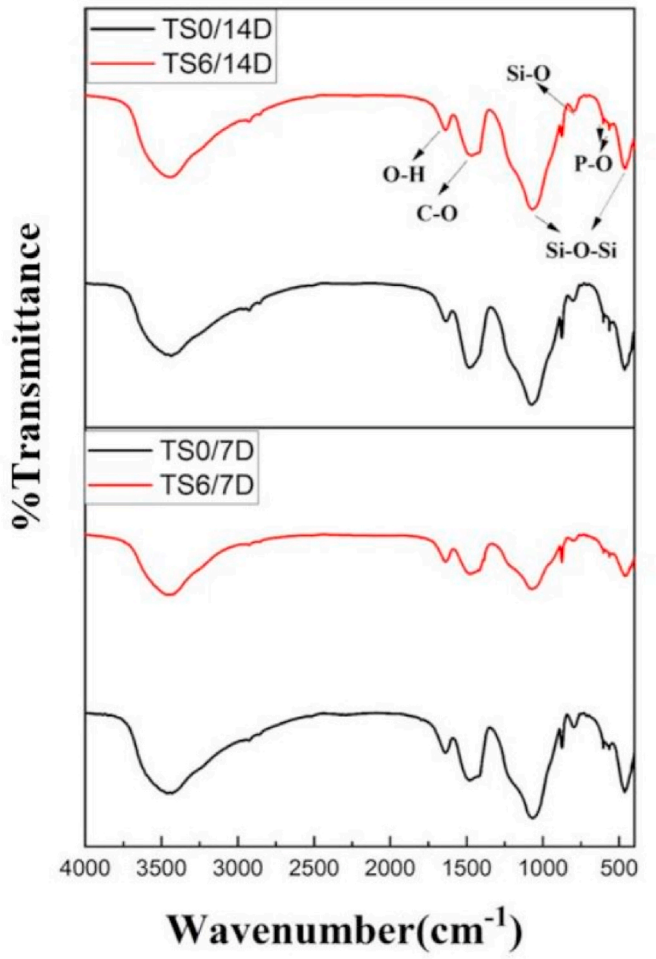

Fig. 3. The FTIR spectra of TS0 and TS6 after soaking in SBF solution for one and two weeks.

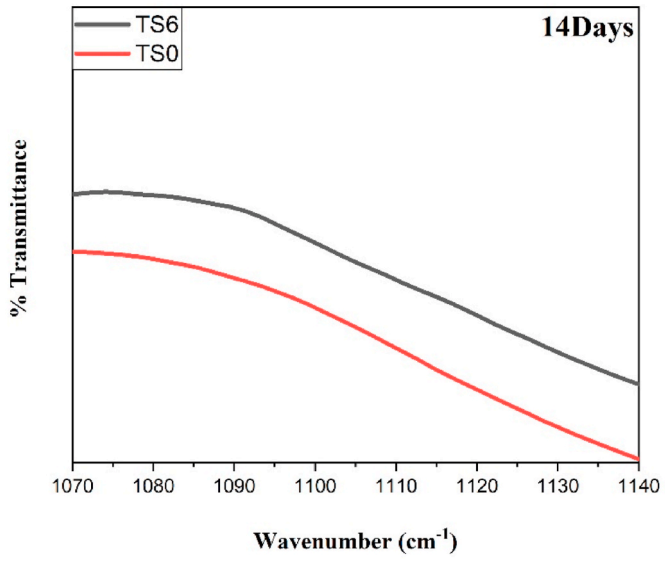

Fig. 4. The FTIR spectra of TS0 and TS6 in the range of 1070–1140 cm^{-1}.

and P elements when they grew [74]. Actually, the increase in Sr concentration was due to more releasing Sr ions in SBF solution due to the lower network connectivity of TS-BGs with more Sr content.

In fact, even though TS12 had the better effect on releasing concentration due to bigger ion radius and increased network disorder, it enhanced the solubility. On the other hand, a higher percentage of Sr can decrease *in vitro* bioactivity and cell proliferation. Therefore, in this research, because the priority was to achieve higher *in vitro* bioactivity and release more Sr ions amounts, the TS6 was considered as the optimal specimen due to its higher *in vitro* HA formation ability.

3.6. pH values

The pH values of TS-BGs can be viewed in Fig. 8. As it was evident, the measuring of pH value was done after 0, 1, 3, 7, and 14 days of soaking in the SBF solution. It should be noted that the increase in the Sr amount led to an increase in pH value in all periods, and also, the rate of pH value changed over time. According to Fig. 8, the rate of increasing pH in the first days of immersion was higher due to the cation change in Ca^{2+} and Sr^{2+} with H^{+} ion, while this rate reduced overtime because when HA formed, the phosphate and carbonate decreased and followed by H^{+} increased. Besides, TS12 showed the upper pH value in all period times in comparison to other TS-BGs. Additionally, it was stated that the pH value of 58S-BG containing Sr was between 7.4 and 8 and confirmed the changing trend [63]. Furthermore, it has been reported that in sol-gel-derived 58S-BG, increasing in Sr amount (5,10 mol. %) increased pH values [10]. In fact, by increasing the Sr amount in TS-BGs, the Ca and Sr ions increased in the solution, that led to increase the pH value. In other words, the increase in Sr ions had an upward effect on increasing pH because of its basicity. Hence, the lowest and highest pH values were attributed to TS0 and TS12, respectively.

3.7. 7. In vitro biological investigation

3.7.1. 7. 1 MTT

The culturing results of MC3T3-E1 osteoblastic cells on TS-BGs are demonstrated in Fig. 9. According to the obtained results, the cell proliferation of specimens altered and enhanced over time. Among of TS-BGs with different Sr amounts, the TS6 exhibited the most significant increase in cell proliferation. In initial immersion time, the difference between TS6 with TS0 and TS12 was slight but, by enhancing soaking time up to two weeks, the difference increased. According to Fig. 9, on the 1st day of immersion, there was a slight difference between specimens ($*p < 0.05$). However, by increasing immersion time until one week, a notable difference was observed between TS6 and TS12 ($**p < 0.01$). Ultimately, after two weeks of soaking, the obtained optical density of TS6 was more significant than TS12 (***p< 0.001), and also a significant difference between TS1 and TS6 was observed (**p< 0.01). Based on previous studies, Hesaraki et al. [75] found that the addition of Sr in a higher amount (7.9 mol. %) in 58S-BG, which was derived by sol-gel method, could inhibit cell growth and proliferation. Furthermore, it was confirmed that cell proliferation increased with the substituted low amount of Sr compared to its high amount. The inhibited effect of the high amount of Sr has also been reported [63]. Moreover, Liu et al. [76] investigated the substituted Sr (0, 1.95, 19.5, and 39 mol. % SrO) in BG, which was synthesized with the melt quench method. The proliferation trend was initially enhanced until BG was substituted with 1.95 mol. % and then declined, and also this trend was repeated in 7, 14, and 21 days. Furthermore, it was observed that the presence of 1 mμ of Sr in the structure led to simulate the proliferation of MC3T3-E1 cells [77].

Altogether, the specific range of Sr substitution in BG could enhance cell proliferation and promoted bone formation more substitution had a

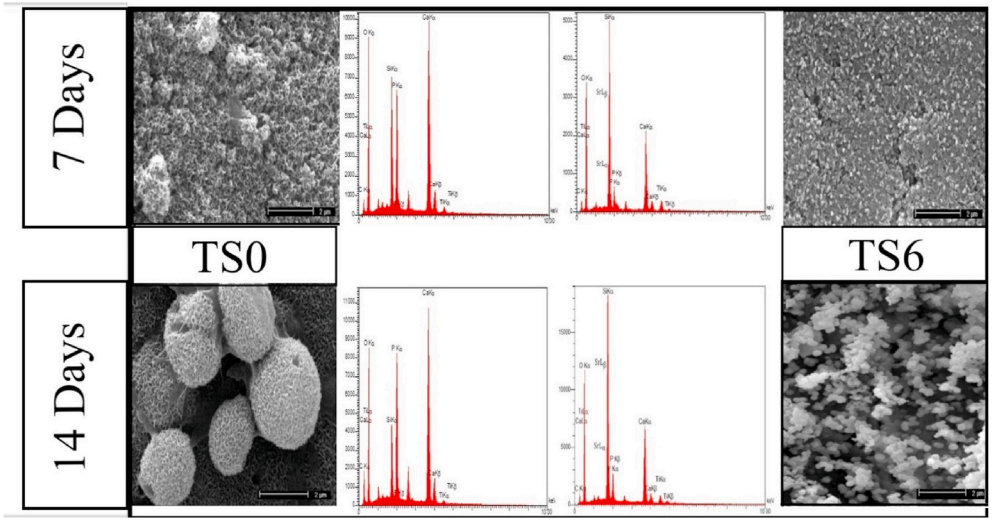

Fig. 5. The SEM images of synthesized TS0 and TS6 surfaces after soaking in SBF solution after one and two weeks.

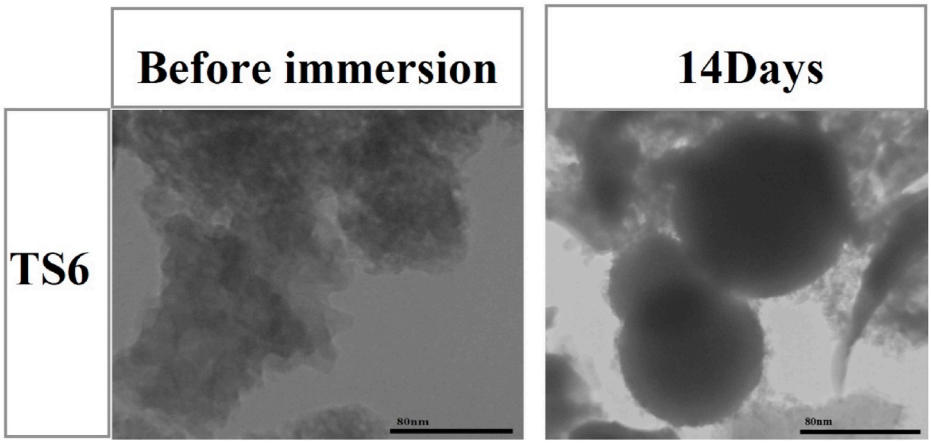

Fig. 6. The TEM image of TS6 before and after soaking for two weeks in the SBF solution.

diverse effect. On the one hand, TS6 displayed better cell proliferation when compared to other specimens. On the other hand, it should be considered that increasing Sr amount diminished the *in vitro* bioactivity. Taken together, TS6 was considered as the optimal specimen in this assay because of the importance of cell proliferation in BGs application.

3.7.2. ALP activity

The activity of MC3T3-E1 cells on TS-BGs was assessed in terms of ALP activity after incubation for 1, 7, and 14 days. Fig. 10 presents the obtained results for ALP activity. It is demonstrated that TS6 had different cell activity concerning other TS-BGs. Additionally, an increasing trend of ALP activity was observed in all period times, but the difference amount became statistically significant by increasing immersion time. The difference of ALP activity between TS0 (BG-free Sr) and TS12 with the highest Sr amount was statistically negligible, but this difference became significant by increasing the immersion period (*$P < 0.05$). According to Fig. 10, on the first day of immersion, there was no appreciable difference between specimens (*$p< 0.05$), but it was observed a significant difference between TS1 and TS6 and TS6 and TS12 as well by increasing immersion time (**$p< 0.01$, * * * $p < 0.001$).

Furthermore, on the last day of immersion, the difference between specimens was similar to the seventh day of immersion. Moreover, Hesaraki et al. [75] confirmed that Sr-substituted 58S-BG enhanced the ALP activity compared to Sr-free BG. Furthermore, it has been reported that substitution of 5 mol. % Sr in 58S-BG led to increasing the ALP activity significantly. Additionally, Capuccini et al. ascertained that increasing Sr amount (Sr substituted HA with different amounts; 0, 1, 3, and 7 atom %) led to enhancing the ALP activity after incubation for 3, 7, 14, and 21 days, and this trend was maximized in 14th day of immersion [57]. Furthermore, Wu et al. [60] reported that the sol-gel derived 64S BG with 5 mol. % Sr showed significantly higher ALP activity when compared to Sr-free glass after 2 and 14 days immersion. According to previous published results and our obtained results in this research, the ALP activity depends on the Sr amount in the crystalline structure (dose-dependant). In other words, as the percentage of Sr increases or decreases, the ALP activity changes. However, according to our obtained ALP activity results, Sr showed the most effect on TS6 and the ALP activity significantly increased in TS6 in comparison to the other TS-BGs.

3.7.3. Antibacterial

A comparative study about the bactericidal efficiency of Sr was carried out on TS-BGs, and the results are illustrated in Fig. 11. As it could be seen, Sr had a significant effect on antibacterial activity, and an

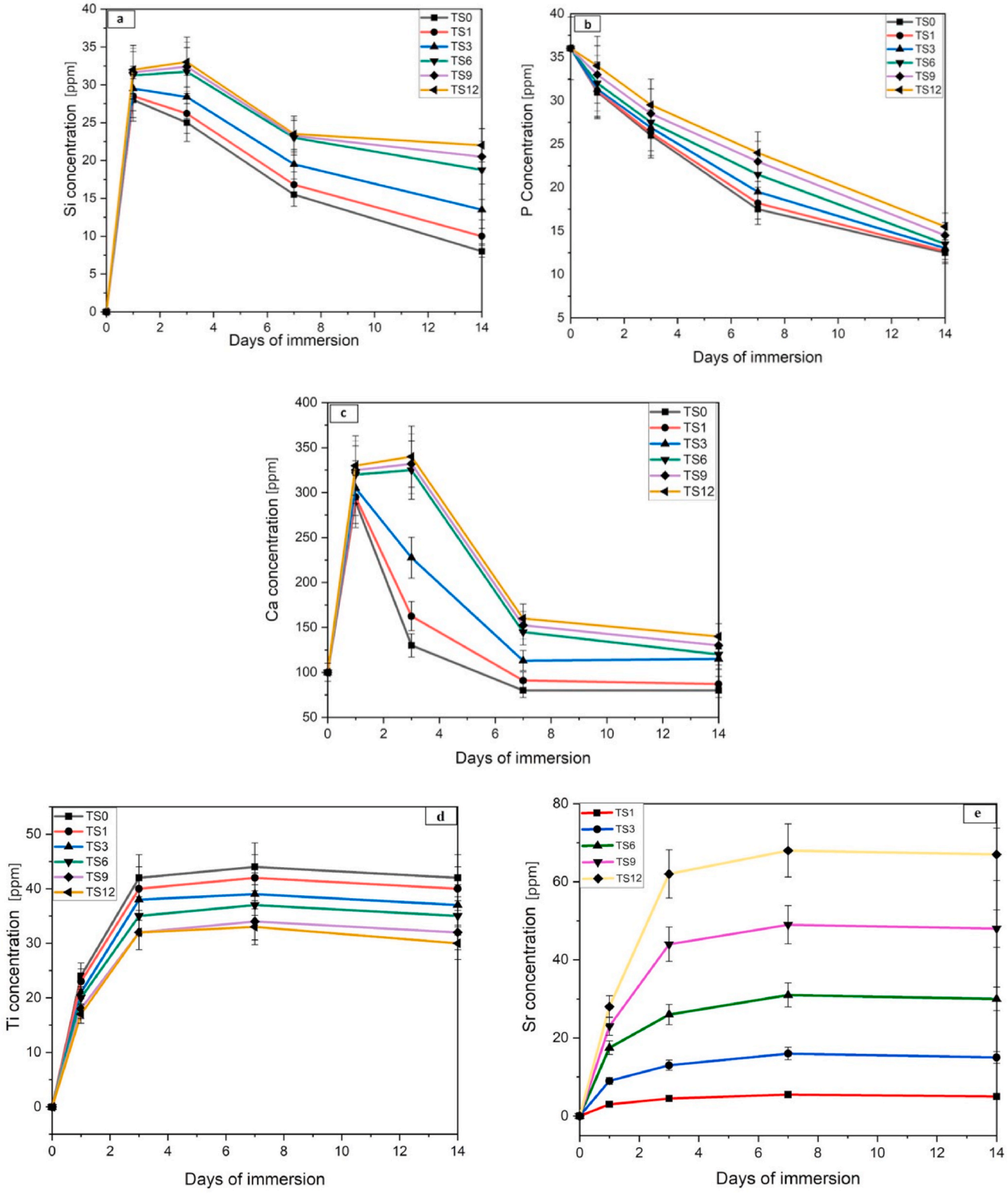

Fig. 7. The concentration of P, Si, Ca, Ti, and Sr ions after soaking in SBF solution after 1, 3, 7, and 14 days.

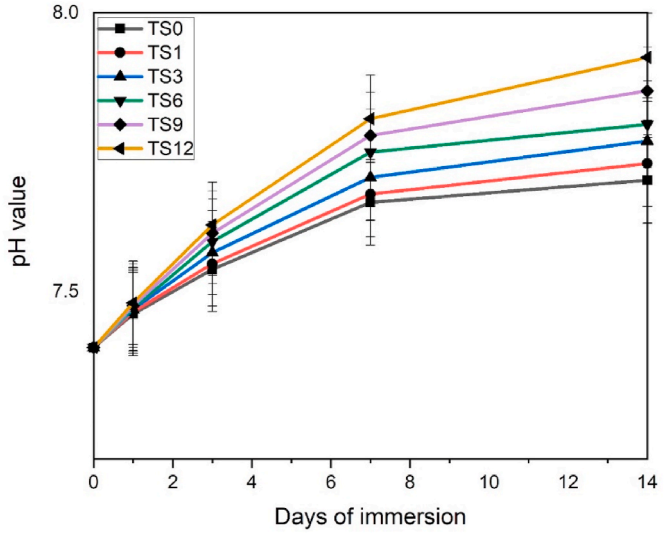

Fig. 8. The pH values of TS-BGs after immersion for 1, 3, 7, and 14 days.

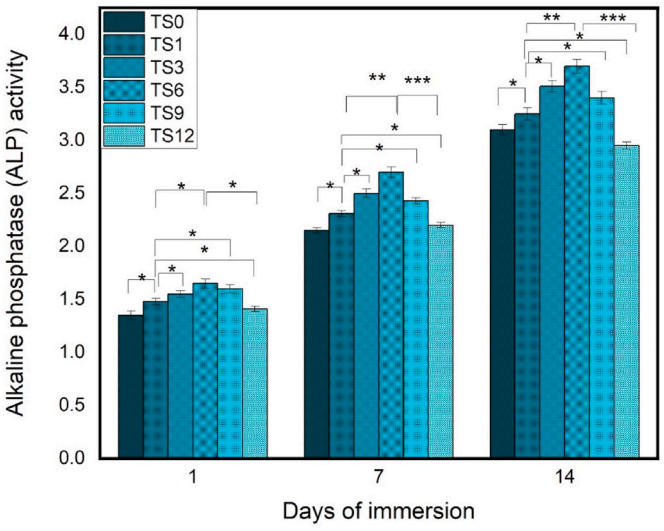

Fig. 10. The ALP activity of TS-BGs after incubation for 1, 7, and 14 days.

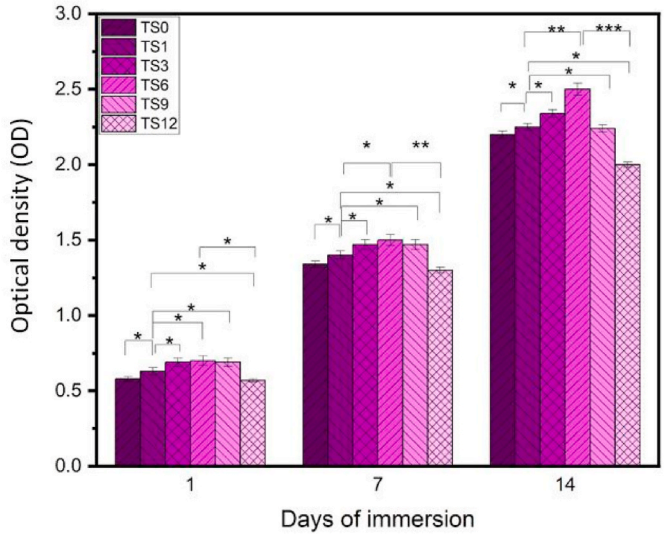

Fig. 9. The MTT activity of synthesized TS-BGs after incubation in SBF solution for 1, 7, and 14 days.

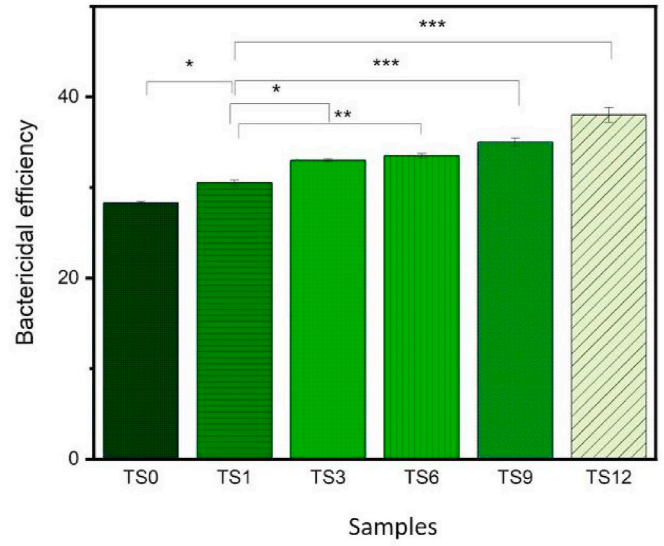

Fig. 11. The bactericidal efficiency of TS-BGs.

increase in Sr amount led to enhance in bactericidal efficiency. Moreover, the simultaneous presence of Sr and Ti improved the antibacterial activity of TS-BGs against bacteria like MRSA. In addition, the difference between TS1 with TS0 and TS3 (*$p < 0.05$) was not noticeable, whiles it was more significant between TS1 with TS6 and TS12 (**$P < 0.01$, * * * $P < 0.001$). It could be seen that by enhancing Sr amount, the bactericidal activity increased, and the number of bacteria decreased. Previous studies noted that by increasing Sr amount in 58S-BG, the bactericidal efficiency enhanced, and BG incorporating 10 mol.% Sr exhibited the highest antibacterial efficiency [63]. Additionally, Liu et al. demonstrated that an increase in the Sr percentage substituted in melt quench derived 42S-BG (1.95, 19.5, and 39 mol. %) led to enhancing bactericidal activity. Also, this activity was significant after incubation for 4 and 6 h in comparison to 2 h incubation [76]. According to previous published research, Sr can be considered as an antibacterial agent, and can resist against different kinds of bacteria as well [78,79].

Furthermore, According to our research, the possible reason for the bactericidal efficiency of Sr was not discovered, but it can be attributed to an increase in Ca, P, and Sr ions releasing and an increase in pH value by increasing Sr amount in all incubation times. Additionally, the hydroxyl group (O–H) as the reactive group was influential on antibacterial activity due to their ability to oxidize the bacteria cell wall. Hence, an increase in Sr amount up to 12 mol.% led to an upward trend in antibacterial activity, and so, TS12 showed 34.27% and 13.43% bactericidal efficiency more than TS0 and TS6, respectively.

4. Supplementary information

The SEM images of synthesized TS-BGs before immersion in SBF solution are illustrated in Fig. 12. Moreover, SEM images of TS0 and TS6 after soaking in SBF solution were shown in Fig. 5. According to the Fig. 12, hydroxyapatite globules were not observed because there was no contact with the SBF solution.

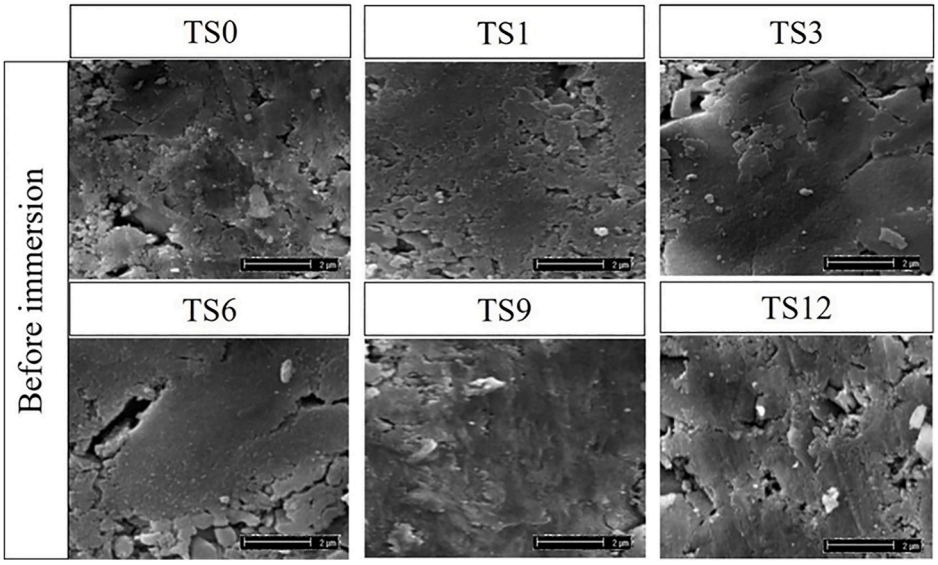

Fig. 12. The SEM images the SEM images of synthesized TS-BGs before immersion in SBF solution.

5. Conclusion

The quaternary silicon-based bioactive glasses were synthesized by adding a fixed 5 mol. % Ti and different Sr percentages in the range of 0, 1, 3, 6, 9, and 12 mol. %. The results are summarized below.

5.1. Structural and morphological results

XRD, FTIR, and SEM analyses were performed on TS-BGs after soaking in SBF solution for one week and two weeks. The obtained results ascertained that by increasing Sr amount, the formed HA amount decreased. Moreover, it was revealed that TS0 exhibited better *in vitro* bioactivity than other specimens, and by increasing the time of immersion, the HA aggregation enhanced. Additionally, the SEM images confirmed HA formation on TS-BGs after soaking in SBF solution for one week and two weeks, and the aggregation of HA globules was more in 14 days immersion. The ICP-AES results exhibited by increasing the Sr amount, the Sr ion releasing increased and this trend was significant after 7 days immersion. Besides, by increasing Sr to composition, the TS-BGs network expanded, and the oxygen density decreased, while the solubility and ion releasing increased.

5.2. Biological properties results

The cell proliferation and growth of MCT3-E1 in contact with TS-BGs showed less cell proliferation, while for TS6 (with a moderate amount of Sr), optical density was the highest. Furthermore, this trend was the same for ALP activity, and among all specimens, TS6 exhibited the highest ALP activity compared to others. However, the antibacterial efficiency trend was different, and by increasing Sr amount, the bactericidal efficiency was enhanced, and the TS12 presented the highest antibacterial activity that was 34.27% more than TS0. Therefore as a conclusion, in the most structural and biological tests, TS6 showed the most effective behavior compared to other TS-BGs, and so, it can be considered as the optimal specimen in the biomedical applications.

Declaration of competing interest

The authors declare that they have no known competing financial interests or personal relationships that could have appeared to influence the work reported in this paper.

References

[1] D. Khorsandi, A. Moghanian, R. Nazari, G. Arabzadeh, S. Borhani, Personalized medicine: regulation of genes in human skin ageing, J. Allergy Ther. 7 (2016) 2–11.
[2] A. Saatchi, A.R. Arani, A. Moghanian, M. Mozafari, Synthesis and characterization of electrospun cerium-doped bioactive glass/chitosan/polyethylene oxide composite scaffolds for tissue engineering applications, J Ceramics International 47 (2020) 260–271.
[3] S. Rahimi, F. SharifianJazi, A. Esmaeilkhanian, M. Moradi, A. Samghabadi, Effect of SiO_2 content on Y-TZP/Al_2O_3 ceramic-nanocomposite properties as potential dental applications, Ceram. Int. 46 (2020) 10910–10916.
[4] M. Shahrbabak, F. Sharifianjazi, D. Rahban, A. Salimi, A comparative investigation on bioactivity and antibacterial properties of sol-gel derived 58S bioactive glass substituted by Ag and Zn, Siliconindia 11 (2019) 2741–2751.
[5] Z. Goudarzi, N. Parvin, F. Sharifianjazi, Formation of hydroxyapatite on surface of SiO_2–P_2O_5–CaO–SrO–ZnO bioactive glass synthesized through sol-gel route, Ceram. Int. 45 (2019) 19323–19330.
[6] R. Nerem, Part H: journal of Engineering in Medicine, Tissue engineering: confronting the transplantation crisis, J.Eng. Med. 214 (2000) 95–99.
[7] E. Sharifi Sedeh, S. Mirdamadi, F. Sharifianjazi, M. Tahriri, Synthesis and evaluation of mechanical and biological properties of scaffold prepared from Ti and Mg with different volume percent, Synthesis and Reactivity in Inorganic, Metal-Organic, Nano-Metal Chemistry 45 (2015) 1087–1091.
[8] P. Abasian, M. Radmansouri, M.H. Jouybari, M.V. Ghasemi, A. Mohammadi, M. Irani, F. Jazi, Incorporation of magnetic NaX zeolite/DOX into the PLA/chitosan nanofibers for sustained release of doxorubicin against carcinoma cells death in vitro, Int. J. Biol. Macromol. 121 (2019) 398–406.
[9] A. Esmaeilkhanian, F. Sharifianjazi, A. Abouchenari, A. Rouhani, N. Parvin, M. Irani, biotechnology, Synthesis and characterization of natural nano-hydroxyapatite derived from Turkey femur-bone waste, J Applied biochemistry and biotechnology 189 (2019) 919–932.
[10] A. Moghanian, S. Firoozi, M. Tahriri, Characterization, in vitro bioactivity and biological studies of sol-gel synthesized SrO substituted 58S bioactive glass, Ceram. Int. 43 (2017) 14880–14890.
[11] A. Pazhouheshgar, S.A.S. Vanini, A. Moghanian, The experimental and numerical study of fracture behavior of 58s bioactive glass/polysulfone composite using the extended finite elements method, Mater. Res. Express 6 (2019), 095208. https://iopscience.iop.org/article/10.1088/2053-1591/ab3495/meta.
[12] A. Pazhouheshgar, A. Moghanian, S.A. Sadough Vanini, The extended finite element method numerical and experimental analysis of mechanical behavior of polysulfone/58s bioactive glass synthesized through solvent casting method, Mod. Mech. Eng. 20 (2020) 2061–2073. https://mme.modares.ac.ir/article -15-37532-en.html.
[13] M. Tahriri, M. Del Monico, A. Moghanian, M.T. Yaraki, R. Torres, A. Yadegari, L. Tayebi, Graphene and its Derivatives: Opportunities and Challenges in Dentistry, vol. 102, 2019, pp. 171–185.
[14] M. Rahmani, A. Moghanian, M. Saghafi Yazdi, The effect of Ag substitution on physicochemical and biological properties of sol-gel derived 60%SiO_2–31% CaO–4%P_2O_5–5%Li_2O (mol%) quaternary bioactive glass, Ceram. Int. 47 (2021) 15985–15994.
[15] L. Hench, The story of Bioglass®, J. Mater. Sci. Mater. Med. 17 (2006) 967–978.
[16] A. Moghanian, M. Zohourfazeli, M.H. Mahdi Tajer, A.K. Miri, Comprehensive *in vitro* studies of novel sol gel-derived Zr^{4+}/Zn^{2+} co-substituted bioactive glass with

enhanced biological properties for bone healing, J. Non-Cryst. Solids 566 (2021) 120887, https://doi.org/10.1016/j.jnoncrysol.2021.120887.
[17] A. Moghanian, M. Zohourfazeli, Investigation the in vitro and bactericidal properties of magnesium and copper containing bioactive glasses, J. Adv. Mater. Technol. 9 (2020) 19–33, https://doi.org/10.30501/JAMT.2020.195763.1041.
[18] A. Moghanian, M. Zohourfazeli, Comparative study on in vitro, physico-chemical and antibacterial properties of 58S and 68S bioactive glasses synthesized by sol-gel method, Adv. Process. Mater. 13 (2020) 17–30. https://www.sid.ir/en/Journal/ViewPaper.aspx?ID=716955.
[19] A. Saatchi, A.R. Arani, A. Moghanian, M. Mozafari, Cerium-doped bioactive glass-loaded chitosan/polyethylene oxide nanofiber with elevated antibacterial properties as a potential wound dressing, Ceram. Int. 47 (2021) 9447–9461.
[20] A. Moghanian, A. Pazhouheshgar, A. Ghorbanoghli, Nonlinear Viscoelastic Modeling of Synthesized Silicate-Based Bioactive Glass/Polysulfone Composite: Theory and Medical Applications, Silicon, 2020, https://doi.org/10.1007/s12633-020-00900-9.
[21] Z. Hajifathali, M. Amirhosseinian, The effect of substitution of CaO/MgO and CaO/SrO on in vitro bioactivity of sol-gel derived bioactive glass, Int. J. Biomed. Biol. Eng. 13 (2019) 279–287.
[22] M. Aminitabar, M. Amirhosseinian, M. Elsa, Synthesis and in vitro characterization of a gel-derived SiO_2-CaO-P_2O_5-SrO-Li_2O bioactive glass, Int. J. Chem. Mol. Eng. 13 (2019) 296–307.
[23] M. Elsa, A. Moghanian, Comparative study of calcium content on in vitro biological and antibacterial properties of silicon-based bioglass, Int. J. Chem. Mol. Eng. 13 (2019) 288–295.
[24] D.C. Coraça-Huber, M. Fille, J. Hausdorfer, D. Putzer, M. Nogler, Efficacy of antibacterial bioactive glass S53P4 against S. aureus biofilms grown on titanium discs in vitro, J. ortho. Res. 32 (2014) 175–177.
[25] N. Li, Q. Jie, S. Zhu, R. Wang, Preparation and characterization of macroporous sol–gel bioglass, Ceram. Int. 31 (2005) 641–646.
[26] A. Moghanian, M. Zohourfazeli, M.H. Tajer, The effect of zirconium content on in vitro bioactivity, biological behavior and antibacterial activity of sol-gel derived 58S bioactive glass, J. Non-Cryst. Solids 546 (2020) 120262.
[27] F. Rupp, L. Liang, J. Geis-Gerstorfer, L. Scheideler, F. Hüttig, Surface characteristics of dental implants: a review, Dent. Mater. 34 (2018) 40–57.
[28] S. Khorsand, M. Fathi, S. Salehi, S. Amirkhanlou, Hydroxyapatite/alumina nanocrystalline composite powders synthesized by sol-gel process for biomedical applications, Int. J. Min. Metal. Mater. 21 (2014) 1033–1036.
[29] M. Kazem-Rostami, A. Moghanian, Hünlich base derivatives as photo-responsive Λ-shaped hinges, J. Org. Chem. Front, 4 (2017) 224–228.
[30] A. Moghanian, R. Portillo-Lara, E. Shirzaei Sani, H. Konisky, S.H. Bassir, N. Annabi, Synthesis and characterization of osteoinductive visible light-activated adhesive composites with antimicrobial properties, J. Tis. Eng. Regen. Med. 14 (2020) 66–81.
[31] A. Moghanian, M.H. Mahdi Tajer, M. Zohourfazeli, Z. Miri, M. Saghafi Yazdi, Sol-gel derived silicate-based bioactive glass: studies of synergetic effect of zirconium and magnesium on structural and biological characteristics, J. Non-Cryst. Solids 554 (2020) 120613, https://doi.org/10.1016/j.jnoncrysol.2020.120613.
[32] A. Moghanian, S. Nasiripour, S. Hosseini, S.M. Hosseini, A. Rashvand, A. Ghorbanoghli, A. Pazhouheshgar, F. Sharifian Jazi, The effect of Ag substitution on physico-chemical and biological propertiesof sol-gel derived 60%SiO_2-31%CaO-4%P_2O_5-5%TiO_2 (mol%) quaternary bioactive glass, J. Non-Cryst. Solids 560 (2021) 120732, https://doi.org/10.1016/j.jnoncrysol.2021.120732.
[33] A.M. El-Kady, A. Ali, Fabrication and characterization of ZnO modified bioactive glass nanoparticles, Ceram. Int. 38 (2012) 1195–1204.
[34] A. Moghanian, S. Firoozi, M. Tahriri, Synthesis and in vitro studies of sol-gel derived lithium substituted 58S bioactive glass, Ceram. Int. 43 (2017) 12835–12843.
[35] A. Moghanian, M. Zohourfazeli, Investigation the in vitro and bactericidal properties of magnesium and copper containing bioactive glasses, J. Adv. Mater. Technol. 9 (2020), https://doi.org/10.30501/JAMT.2020.195763.1041, 1–15.
[36] A. Moghanian, A. Koohfar, S. Hosseini, S. Hosseini, A. Ghorbanoghli, M. Sajjadnejad, M. Raz, M. Elsa, F. Sharifian Jazi, Synthesis, characterization and in vitro biological properties ofsimultaneous co-substituted Ti^{+4}/Li^{+1} 58s bioactive glass, J. Non-Cryst. Solids 561 (2021) 120740, https://doi.org/10.1016/j.jnoncrysol.2021.120740.
[37] A. Moghanian, M. Zohourfazeli, M.H. Mahdi Tajer, Z. Miri, S. Hosseini, A. Rashvand, Preparation, characterization and in vitro biological response of simultaneous co-substitution of Zr^{+4}/Sr^{+2} 58S bioactive glass powder, Ceram. Int. (2020), https://doi.org/10.1016/j.ceramint.2020.11.139.
[38] M. Niinomi, C. Boehlert, Titanium alloys for biomedical applications. Advances in Metallic Biomaterials, Springer, 2015, pp. 179–213.
[39] M. Zohourfazeli, M.H. Mahdi Tajer, A. Moghanian, Comprehensive investigation on multifunctional properties of zirconium and silver co-substituted 58S bioactive glass, Ceram. Int. 47 (2021) 2499–2507.
[40] Y. Song ab, D.S. Xu a, R. Yang a, D. Li a, W.T. Wub, Z.X. Guo, Theoretical study of the effects of alloying elements on the strength and modulus of β-type bio-titanium alloys, J. Mater. Sci. Eng. 260 (1999) 269–274.
[41] B.A. Ben-Arfa, I. Salvado, J.M. Ferreira, R. Pullar, The effect of functional ions (Y^{3+}, F^{-}, Ti^{4+}) on the structure, sintering and crystallization of diopside-calcium pyrophosphate bioglasses, J. Non-Cryst. Solids 443 (2016) 162–171.
[42] S. Heidari, T. Hooshmand, B.E. Yekta, A. Tarlani, N. Noshiri, M. Tahriri, Effect of addition of titanium on structural, mechanical and biological properties of 45S5 glass-ceramic, J Ceramics International 44 (2018) 11682–11692.
[43] A. Moghanian, S. Nasiripour, A. Koohfar, M. Sajjadnejad, S.M. Hosseini, M. Taherkhani, Z. Miri, S.H. Hosseini, M. Aminitabar, A. Rashvand, Characterization, in vitro bioactivity and biological studies of sol-gel-derived TiO_2 substituted 58S bioactive glass, J Applied Ceramic Technology, 2021, https://doi.org/10.1111/ijac.13782.
[44] S.M. Rabiee, N. Nazparvar, M. Azizian, D. Vashaee, L. Tayebi, Effect of ion substitution on properties of bioactive glasses: a review, J. Cer. Int. 41 (2015) 7241–7251.
[45] S. Fiorilli, G. Molino, C. Pontremoli, G. Iviglia, E. Torre, C. Cassinelli, M. Morra, C. Vitale-Brovarone, The incorporation of strontium to improve bone-regeneration ability of mesoporous bioactive glasses, Materials 11 (2018) 678, https://doi.org/10.3390/ma11050678.
[46] S.K. Arepalli, H. Tripathi, S.K. Hira, P.P. Manna, R. Pyare, S.J. Singh, Enhanced bioactivity, biocompatibility and mechanical behavior of strontium substituted bioactive glasses, J. Mater. Sci. Eng. C 69 (2016) 108–116.
[47] F. Sharifianjazi, M. Moradi, A. Abouchenari, A.H. Pakseresht, A. Esmaeilkhanian, M. Shokouhimehr, M. Asl, Effects of Sr and Mg dopants on biological and mechanical properties of SiO_2–CaO–P_2O_5 bioactive glass, J. Cer. Int. 46 (2020) 22674–22682.
[48] D. Sriranganathan, N. Kanwal, K.A. Hing, R.G. Hill, Strontium substituted bioactive glasses for tissue engineered scaffolds: the importance of octacalcium phosphate, J. Mater. Sci. Mater. Med. 27 (2016) 39, https://doi.org/10.1007/s10856-015-5653-6.
[49] B.F. Dizaji, M.H. Azerbaijan, N. Sheisi, P. Goleij, T. Mirmajidi, F. Chogan, M. Irani, F. Sharafian, Synthesis of PLGA/chitosan/zeolites and PLGA/chitosan/metal organic frameworks nanofibers for targeted delivery of Paclitaxel toward prostate cancer cells death, Int. J. Biol. Macromol. 164 (2020) 1461–1474.
[50] N.P. Vitko, A. Richardson, Laboratory maintenance of methicillin-resistant Staphylococcus aureus (MRSA), J. Current prot. Microbiol. 28 (2013), 9C. 2.1-9C. 2.14.
[51] M.C. Enright, D.A. Robinson, G. Randle, E.J. Feil, H. Grundmann, B. Spratt, The evolutionary history of methicillin-resistant Staphylococcus aureus (MRSA), J. Proc. Nat. Acad. Sci. 99 (2002) 7687–7692.
[52] F. Sharifianjazi, N. Parvin, M. Tahriri, Synthesis and characteristics of sol-gel bioactive SiO_2-P_2O_5-CaO-Ag_2O glasses, J. Non-Cryst. Solids 476 (2017) 108–113.
[53] M. Radmansouri, E. Bahmani, E. Sarikhani, K. Rahmani, F. Sharifianjazi, M. Irani, Doxorubicin hydrochloride-Loaded electrospun chitosan/cobalt ferrite/titanium oxide nanofibers for hyperthermic tumor cell treatment and controlled drug release, Int. J. Biol. Macromol. 116 (2018) 378–384.
[54] F.S. Jazi, N. Parvin, M. Rabiei, M. Tahriri, Z.M. Shabestari, A. Azadmehr, Effect of the synthesis route on the grain size and morphology of ZnO/Ag nanocomposite, J. Ceramic Proc. Res. 13 (2012) 523–526.
[55] E. Abou Neel, W. Chrzanowski, D. Pickup, L. O'Dell, N. Mordan, R. Newport, M. Smith, J. Knowles, Structure and properties of strontium-doped phosphate-based glasses, J. R. Soc. Interface 6 (2009) 435–446.
[56] E. Gentleman, Y.C. Fredholm, G. Jell, N. Lotfibakhshaiesh, M. O'Donnell, R. Hill, M. Stevens, The effects of strontium-substituted bioactive glasses on osteoblasts and osteoclasts in vitro, J. Biomater. 31 (2010) 3949–3956.
[57] C. Capuccini, P. Torricelli, E. Boanini, M. Gazzano, R. Giardino, A. Bigi, The Japanese Society for Biomaterials, Interaction of Sr-doped hydroxyapatite nanocrystals with osteoclast and osteoblast-like cells, J. Biomed. Mater. Res. 89 (2009) 594–600.
[58] F. Yang, D. Yang, J. Tu, Q. Zheng, L. Cai, L. Wang, Strontium enhances osteogenic differentiation of mesenchymal stem cells and in vivo bone formation by activating Wnt/catenin signaling, J. Stem Cell. 29 (2011) 981–991.
[59] Y. Li, A. Matinmanesh, D.J. Curran, E.H. Schemitsch, P. Zalzal, M. Papini, A. W. Wren, M. Towler, Characterization and fracture property of different strontium-containing borate-based glass coatings for Ti6Al4V substrates, J. Non-Cryst. Solids 458 (2017) 69–75.
[60] X. Wu, G. Meng, S. Wang, F. Wu, W. Huang, Z. Gu, Zn and Sr incorporated 64S bioglasses: material characterization, in-vitro bioactivity and mesenchymal stem cell responses, J. Mater. Sci. Eng. 52 (2015) 242–250.
[61] T. Kokubo, Bioactive glass ceramics: properties and applications, Biomaterials 12 (1991) 155–163.
[62] A. Oliveira, R. Reis, P. Li, Strontium-substituted apatite coating grown on Ti6Al4V substrate through biomimetic synthesis, J. Biomed. Mater. Res. 83 (2007) 258–265.
[63] A. Moghanian, S. Firoozi, M. Tahriri, A. Sedghi, A comparative study on the in vitro formation of hydroxyapatite, cytotoxicity and antibacterial activity of 58S bioactive glass substituted by Li and Sr, Mater. Sci. Eng. 91 (2018) 349–360.
[64] A. Moghanian, A. Ghorbanoghli, M. Kazem-Rostami, A. Pazhouheshgar, E. Salari, M. Saghafi Yazdi, T. Alimardani, H. Jahani, F. Sharifian Jazi, M. Tahriri, Novel antibacterial Cu/Mg-substituted 58S-bioglass: synthesis, characterization and investigation of in vitro bioactivity, Int. J. Appl. Glass Sci. (2019).
[65] S. Hu, C. Ning, Y. Zhou, L. Chen, K. Lin, J. Chang, J of Wuhan University of Technology-Mater. Sci. Ed. Antibacterial Activity of Silicate Bioceramics vol. 26, 2011, pp. 226–230.
[66] A. Moghanian, A. Sedghi, A. Ghorbanoghli, E. Salari, The effect of magnesium content on in vitro bioactivity, biological behavior and antibacterial activity of sol–gel derived 58S bioactive glass, Ceram. Int. 44 (2018) 9422–9432.
[67] M. Tylkowski, D. Brauer, Mixed alkali effects in Bioglass® 45S5, J. Non-Cryst. Solids 376 (2013) 175–181.
[68] R. Brückner, M. Tylkowski, L. Hupa, D. Brauer, Controlling the ion release from mixed alkali bioactive glasses by varying modifier ionic radii and molar volume, J. Mater. Chem. B 4 (2016) 3121–3134.
[69] Z. Zhong, J. Qin, J. Ma, Electrophoretic deposition of biomimetic zinc substituted hydroxyapatite coatings with chitosan and carbon nanotubes on titanium, J Ceramics International 41 (2015) 8878–8884.

[70] A. Hoppe, B. Sarker, R. Detsch, N. Hild, D. Mohn, W.J. Stark, A.R. Boccaccini, In vitro reactivity of Sr-containing bioactive glass (type 1393) nanoparticles, J. Non-Cryst. Solids 387 (2014) 41–46.
[71] D. Farlay, G. Panczer, C. Rey, P.D. Delmas, G. Boivin, Mineral maturity and crystallinity index are distinct characteristics of bone mineral, J. Bone Miner. Metabol. 28 (2010) 433–445.
[72] A. Goel, R.R. Rajagopal, J.M.J.A.B. Ferreira, Influence of strontium on structure, sintering and biodegradation behaviour of CaO–MgO–SrO–SiO_2–P2O5–CaF_2 glasses, Acta Biomater. 7 (2011) 4071–4080.
[73] V. Aina, L. Bergandi, G. Lusvardi, G. Malavasi, F.E. Imrie, I.R. Gibson, G. Cerrato, D.J. Ghigo, E. C, Sr-containing hydroxyapatite: morphologies of HA crystals and bioactivity on osteoblast cells, Mater. Sci. Eng. 33 (2013) 1132–1142.
[74] S. Hesaraki, M. Alizadeh, H. Nazarian, D.J. Sharifi, Physico-chemical and in vitro biological evaluation of strontium/calcium silicophosphate glass, J. Mater. Sci. Mater. Med. 21 (2010) 695–705.
[75] S. Hesaraki, M. Gholami, S. Vazehrad, S. Shahrabi, E. C, The effect of Sr concentration on bioactivity and biocompatibility of sol–gel derived glasses based on CaO–SrO–SiO_2–P_2O_5 quaternary system, J. Mater. Sci. Eng. 30 (2010) 383–390.
[76] J. Liu, S.C. Rawlinson, R.G. Hill, F. Fortune, Strontium-substituted bioactive glasses in vitro osteogenic and antibacterial effects, J Dental Materials 32 (2016) 412–422.
[77] N. Chattopadhyay, S.J. Quinn, O. Kifor, C. Ye, E. Brown, The calcium-sensing receptor (CaR) is involved in strontium ranelate-induced osteoblast proliferation, Biochem. Pharmacol. 74 (2007) 438–447.
[78] N.D. Ravi, R. Balu, T. Sampath Kumar, Strontium-substituted calcium deficient hydroxyapatite nanoparticles: synthesis, characterization, and antibacterial properties, J. Am. Ceram. Soc. 95 (2012) 2700–2708.
[79] A. Wren, A. Coughlan, M. Hall, M. German, M. Towler, Comparison of a SiO_2–CaO–ZnO–SrO glass polyalkenoate cement to commercial dental materials: ion release, biocompatibility and antibacterial properties, J. Mater. Sci.: Mater. Med. 24 (2013) 2255–2264.